

# UC Berkeley

## Research Reports

### Title

Fault Detection And Identification With Application To Advanced Vehicle Control Systems

### Permalink

<https://escholarship.org/uc/item/1jb6z0qm>

### Authors

Douglas, Randal K.

Chung, Walter H.

Malladi, Durga P.

et al.

### Publication Date

1997

CALIFORNIA PATH PROGRAM  
INSTITUTE OF TRANSPORTATION STUDIES  
UNIVERSITY OF CALIFORNIA, BERKELEY

## **Development of Binocular Stereopsis for Vehicle Lateral Control, Longitudinal Control and Obstacle Detection**

**Jitendra Malik, Camillo J. Taylor,  
Philip McLauchlan, Jana Kosecka**

**California PATH Research Report  
UCB-ITS-PRR-97-41**

This work was performed as part of the California PATH Program of the University of California, in cooperation with the State of California Business, Transportation, and Housing Agency, Department of Transportation; and the United States Department of Transportation, Federal Highway Administration.

The contents of this report reflect the views of the authors who are responsible for the facts and the accuracy of the data presented herein. The contents do not necessarily reflect the official views or policies of the State of California. This report does not constitute a standard, specification, or regulation.

Report for MOU 257

November 1997

ISSN 1055-1425

**Fault Detection and Identification  
With Application to  
Advanced Vehicle Control Systems**

Randal K. Douglas, Walter H. Chung, Durga P. Malladi, Robert H. Chen,  
Jason L. Speyer and D. Lewis Mingori

Mechanical and Aerospace Engineering Department  
University of California, Los Angeles  
Los Angeles, California 90095



# **Fault Detection and Identification With Application to Advanced Vehicle Control Systems**

**Randal K. Douglas, Walter H. Chung, Durga P. Malladi,  
Robert H. Chen, Jason L. Speyer and D. Lewis Mingori**

Mechanical and Aerospace Engineering Department  
University of California, Los Angeles  
Los Angeles, California 90095

December 5, 1997



# Fault Detection and Identification With Application to Advanced Vehicle Control Systems

Randal K. Douglas, Walter H. Chung, Durga P. Malladi, Robert H. Chen, Jason L. Speyer  
and D. Lewis Mingori

*Mechanical and Aerospace Engineering Department  
University of California, Los Angeles  
Los Angeles, California 90095*

December 5, 1997

## Abstract

This report is a continuation of the work of (Douglas et al. 1996) in which a preliminary design of a health monitoring system for automated vehicles is described. The approach is to fuse data from dissimilar instruments using modeled dynamic relationships and fault detection and identification filters. The filters are constructed so that the residual process has static directional characteristics associated with the presence of a fault. Refinements to the residual generation scheme are described that bring our systems in closer alignment with the needs of the U.C. Berkeley group. Eleven sensors and two actuators associated with the longitudinal dynamics are now considered and hardware redundancy is taken into account.

**Keywords.** Automated Highway Systems, Automatic Vehicle Monitoring, Fault Detection and Fault Tolerant Control, Reliability, Sensors, Vehicle Monitoring.





# **Fault Detection and Identification With Application to Advanced Vehicle Control Systems**

M.O.U. 241

## **Executive Summary**

This report is a continuation of the work of (Douglas et al. 1996) in which a preliminary design of a health monitoring system for automated vehicles is described. The approach is to fuse data from dissimilar instruments using modeled dynamic relationships and fault detection and identification filters. The filters are constructed so that the residual process has static directional characteristics associated with the presence of a fault. Refinements to the residual generation scheme are described that bring our systems in closer alignment with the needs of the U.C. Berkeley group. Eleven sensors and two actuators associated with the longitudinal dynamics are now considered and hardware redundancy is taken into account.



# Contents

---

|   |            |
|---|------------|
| <b>Abstract</b> . . . . .                                     | <b>v</b>   |
| <b>Executive Summary</b> . . . . .                            | <b>vii</b> |
| <b>List of Figures</b> . . . . .                              | <b>xi</b>  |
| <b>Chapter 1 Introduction</b> . . . . .                       | <b>1</b>   |
| <b>Chapter 2 Vehicle Model</b> . . . . .                      | <b>5</b>   |
| 2.1 Linear Model . . . . .                                    | 6          |
| 2.1.1 Linear Model Reduction . . . . .                        | 7          |
| 2.1.2 Vehicle Measurements . . . . .                          | 8          |
| 2.2 Suspension Model . . . . .                                | 9          |
| 2.2.1 Suspension Model With Suspension Length State . . . . . | 10         |
| 2.2.2 Suspension Model With Suspension Force State . . . . .  | 11         |
| 2.2.3 Example . . . . .                                       | 13         |
| 2.3 Manifold Temperature Model . . . . .                      | 14         |

---

|                                  |  |           |
|----------------------------------|--|-----------|
| <b>Chapter 3</b>                 | <b>Fault Detection By Analytic Redundancy</b>        | <b>15</b> |
| 3.1                              | Analytic Redundancy                                  | 16        |
| 3.1.1                            | Beard-Jones Fault Detection Filter Background        | 17        |
| 3.1.2                            | Fault Modelling                                      | 19        |
| 3.1.3                            | Special Design Considerations                        | 21        |
| Ill-conditioned fault direction  |  | 21        |
| Output separability              |  | 21        |
| Zero steady-state fault residual |  | 23        |
| 3.1.4                            | Fault Assignment to Multiple Fault Detection Filters | 25        |
| 3.1.5                            | Fault Detection Filter Design For Sensors            | 28        |
| 3.1.6                            | Fault Detection Filter Design For Actuators          | 33        |
| 3.2                              | Algebraic Redundancy                                 | 35        |
| 3.3                              | Structure  | 36        |
| <b>Chapter 4</b>                 | <b>Conclusions</b>                                   | <b>39</b> |
| <b>Appendix A</b>                | <b>Fault Detection Filter Design Data</b>            | <b>41</b> |
| <b>References</b>                |  | <b>45</b> |

# List of Figures

---

Figure 1.1 A System View of Vehicle Health Management . . . . . 2

Figure 2.1 Simplified suspension and tire model . . . . . 9

Figure 3.1 Fault Signatures . . . . . 23

Figure 3.2 Fault Signatures . . . . . 25

Figure 3.3 Fault Signatures . . . . . 26

Figure 3.4 Singular value frequency response from all faults to throttle residual . . 35

Figure 3.5 Fault Signatures . . . . . 37



## CHAPTER 1

# Introduction

---

THIS REPORT is a continuation of the work of (Douglas et al. 1996) in which a preliminary design of a health monitoring system for automated vehicles is described. A system view of vehicle health management is summarized by Figure 1.1. Vehicle dynamics are driven by throttle, brake and steering commands and various unmeasured exogenous influences such as road variations and wind and faults. Sensors measure a possible nonlinear function of the dynamic states and are corrupted by noise, biases and faults of their own. A fault detection module uses the sensor measurements and known dynamic inputs to produce a conditional probability of a fault hypothesis. The fault hypothesis is generated in two stages. First, a residual generator formed as a combination of linear observers and algebraic parity equations produces a static pattern uniquely identified with a given fault or no-fault condition. Since the static patterns are only clearly identifiable in nominal operating conditions, the second stage, a residual processor, interrogates the residual and matches it to one of many known patterns. The pattern matching is done with a probabilistically based algorithm so the

residual processor produces a fault hypothesis probability rather than a simple binary announcement. A simple threshold mapping could be added very easily to produce a binary announcement if that were needed. A fault hypothesis probability is passed to a vehicle health monitoring and reconfiguration system. These components determine the impact of the possible fault on safe vehicle operation and adjust control laws if necessary to accommodate a degraded operating condition. These components are being developed by the UC Berkeley team.

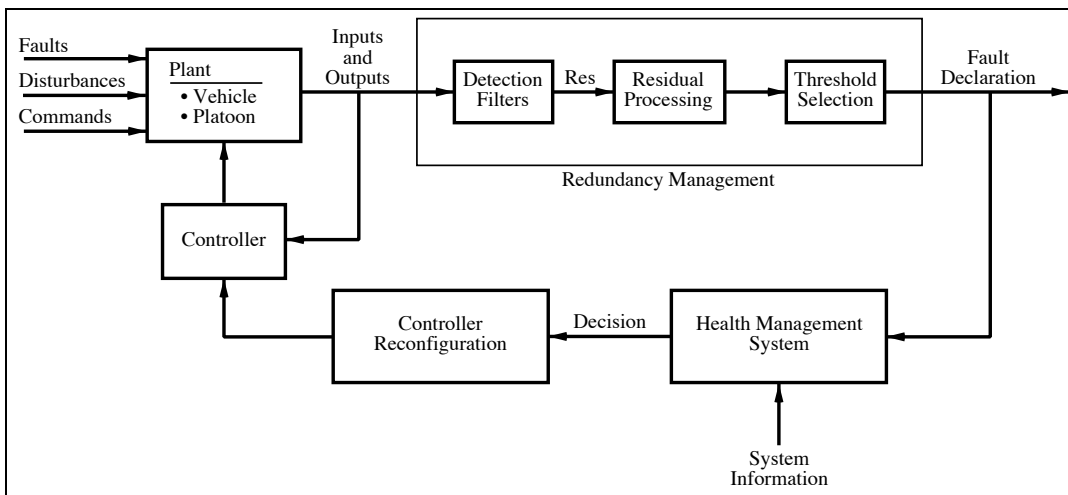


Figure 1.1: A System View of Vehicle Health Management.

Chapters 2 and 3 describe a residual generator that is designed as a component of a fault detection and identification module in a comprehensive health monitoring and reconfiguration system under development at UC Berkeley. The system is a point design. It is designed to detect faults in eleven sensors and two actuators associated with the longitudinal motion of the modeled vehicle. The vehicle has a nominal operating speed of 25 meters per second on a straight pathway. The nonlinear vehicle and road model used for simulation and the reduced-order linear models used for fault detection filter design are described in Chapter 2. The fault detection filter design is discussed in Chapter 3. An evaluation of the performance of the fault detection filters is deferred to the final report for PATH MOU 291 (Douglas et al. 1997). A residual processor design based on a multiple



hypothesis Shiriyayev sequential probability ratio test is also described there. Finally, for continuity, all material presented in this report is also given in (Douglas et al. 1997).



## CHAPTER 2

# Vehicle Model

---

IN THIS CHAPTER, vehicle models are developed for the design and evaluation of fault detection filters. A high-fidelity six degree of freedom nonlinear vehicle model described in last year's report (Douglas et al. 1996) allows for arbitrary variations in road slope and road noise. An object-oriented vehicle simulation is implemented in C++ and is currently hosted on an Apple Macintosh PowerPC 8100 computer.

Linear models for the longitudinal vehicle dynamics are derived numerically from the nonlinear vehicle simulation using a central differences method. The models are described in Section 2.1 and the derivation method is described in (Douglas et al. 1996). Model order reduction issues related to the suspension model are discussed in Section 2.2.

The manifold temperature measurement model is discussed in Section 2.3. To monitor the health of the manifold temperature sensor, an analytically redundant relationship for the manifold temperature has to be found. Since the temperature enters the engine model as a constant, a state model would introduce an unobservable integrator. An alternative is to let the temperature be a known, that is measured, input to the engine.

## 2.1 Linear Model

The linearized longitudinal dynamics of the vehicle are derived numerically from high-fidelity nonlinear simulation using a central differences method. The nonlinear model and the central differences method are described in detail in (Douglas et al. 1996). The linearization is done at a single nominal operating point of 25 meters per second, about 56 miles per hour, where the car is travelling straight ahead. Since the car is not in a turn, the linear longitudinal dynamics decouple completely from the linear lateral dynamics. The longitudinal model has thirteen states and three inputs. Two of the inputs, throttle and brake actuator commands are regarded as controls. The third input is the manifold temperature and is regarded as a known, that is measured, exogenous input.

|                 |   |
|-----------------|---|
| States:         | $m_a$ : Manifold air mass.                    |
|                 | $\omega_e$ : Engine speed.                    |
|                 | $v_x$ : Longitudinal velocity.                |
|                 | $z$ : Vertical position.                      |
|                 | $v_z$ : Vertical velocity.                    |
|                 | $\theta$ : Pitch angle.                       |
|                 | $q$ : Pitch rate.                             |
|                 | $\bar{\omega}_f$ : Sum of front wheel speeds. |
|                 | $\bar{\omega}_r$ : Sum of rear wheel speeds.  |
|                 | $\bar{F}_f$ : Sum of front suspension forces. |
|                 | $\bar{F}_r$ : Sum of rear suspension forces.  |
|                 | $\alpha$ : Throttle state.                    |
|                 | $T_b$ : Brake state.                          |
| Control inputs: | $u_\alpha$ : Throttle command.                |
|                 | $u_{T_b}$ : Brake command.                    |

Exogenous input:  $\omega_{T_m}$  : Manifold temperature.

The lateral model states and inputs are given for completeness although they are not used.

States:  $v_y$  : Lateral velocity.  
 $\phi$  : Roll angle.  
 $p$  : Roll rate.  
 $r$  : Yaw rate.  
 $\tilde{\omega}_f$  : Difference of front wheel speeds.  
 $\tilde{\omega}_r$  : Difference of rear wheel speeds.  
 $\tilde{F}_f$  : Difference of front suspension forces.  
 $\tilde{F}_r$  : Difference of rear suspension forces.  
 $\gamma$  : Steering state.

Control inputs:  $u_\gamma$  : Steering command.

### 2.1.1 Linear Model Reduction

The thirteenth-order longitudinal model has eigenvalues:  $-215.62$ ,  $-160.79$ ,  $-136.03 \pm 1.67i$ ,  $-90.91$ ,  $-31.56$ ,  $-26.26$ ,  $-2.00 \pm 6.55i$ ,  $-1.32 \pm 5.56i$ ,  $-1.25$  and  $-0.0418$ . Observe that five of these eigenvalues are significantly faster than the rest. By inspection of the eigenvectors, it is determined that the fast eigenvalues are associated with the states  $\bar{\omega}_f$ ,  $\bar{\omega}_r$ ,  $\bar{F}_f$ ,  $\bar{F}_r$  and  $\alpha$ .

A model order reduction is done by dynamic truncation with a steady-state correction. First, the derivatives of the fast states  $\bar{\omega}_f$ ,  $\bar{\omega}_r$ ,  $\bar{F}_f$ ,  $\bar{F}_r$  and  $\alpha$  are set to zero. Then, the linear dynamic equations are solved for the fast states in terms of the remaining states:  $m_a$ ,  $\omega_e$ ,  $v_x$ ,  $z$ ,  $v_z$ ,  $\theta$ ,  $q$  and  $T_b$ . The result is substituted into the state equations of the remaining states. This process is described in more detail in Section 2.3 of (Douglas et al. 1996). The eigenvalues of the eighth-order reduced-order longitudinal model are  $-33.01$ ,  $-25.87$ ,  $-2.08 \pm 6.45i$ ,  $-1.44 \pm 5.47i$ ,  $-1.25$  and  $-0.0451$  which are close to the eigenvalues of the

full-order longitudinal model. Also the frequency responses of the reduced and full-order models are close to each other.

The reduced-order linear longitudinal dynamics data are given in Appendix A.

### 2.1.2 Vehicle Measurements

There are thirteen sensors on the car.

$y_{m_a}$  : Manifold air mass sensor.

$y_{\omega_e}$  : Engine speed sensor.

$y_{T_m}$  : Manifold temperature sensor.

$y_{p_m}$  : Manifold pressure sensor.

$y_{v_x}$  : Longitudinal velocity sensor.

$y_{a_x}$  : Longitudinal accelerometer.

$y_{a_z}$  : Vertical accelerometer.

$y_{\omega_{fl}}$  : Front left wheel speed sensor.

$y_{\omega_{fr}}$  : Front right wheel speed sensor.

$y_{\omega_{rl}}$  : Rear left wheel speed sensor.

$y_{\omega_{rr}}$  : Rear right wheel speed sensor.

$y_{\alpha}$  : Throttle sensor.

$y_{T_b}$  : Brake sensor.

Since the dynamics naturally decompose into longitudinal and lateral components, the following processed wheel speed sensors form a more natural set of measurements:

$y_{\bar{\omega}_f}$  : Sum of front wheel speeds.

$y_{\bar{\omega}_r}$  : Sum of rear wheel speeds.

$y_{\tilde{\omega}_f}$  : Difference of front wheel speeds.

$y_{\tilde{\omega}_r}$  : Difference of rear wheel speeds.

For the longitudinal dynamics, the wheel speed difference sensors  $y_{\bar{\omega}_f}$  and  $y_{\bar{\omega}_r}$  are not relevant. Also, the throttle and brake sensors  $y_{\alpha}$  and  $y_{T_b}$  measure control inputs rather than states. The manifold temperature sensor  $y_{T_m}$  measures an exogenous input. Finally, the manifold pressure  $y_{p_m}$  and manifold air mass  $y_{m_a}$  are linearly dependent. Thus, there are only seven sensors that provide measurements linearly related to the vehicle longitudinal states:  $y_{m_a}$ ,  $y_{\omega_e}$ ,  $y_{v_x}$ ,  $y_{a_x}$ ,  $y_{a_z}$ ,  $y_{\bar{\omega}_f}$  and  $y_{\bar{\omega}_r}$ .

The reduced-order linear longitudinal measurement data are given in Appendix A.

## 2.2 Suspension Model

The suspension system is modelled as a nonlinear spring and linear damper. The tire is a mass and linear spring. Since the mass of the tire is very small relative to the car, the tire model is simplified to a linear spring as shown in Figure 2.1. It is possible to

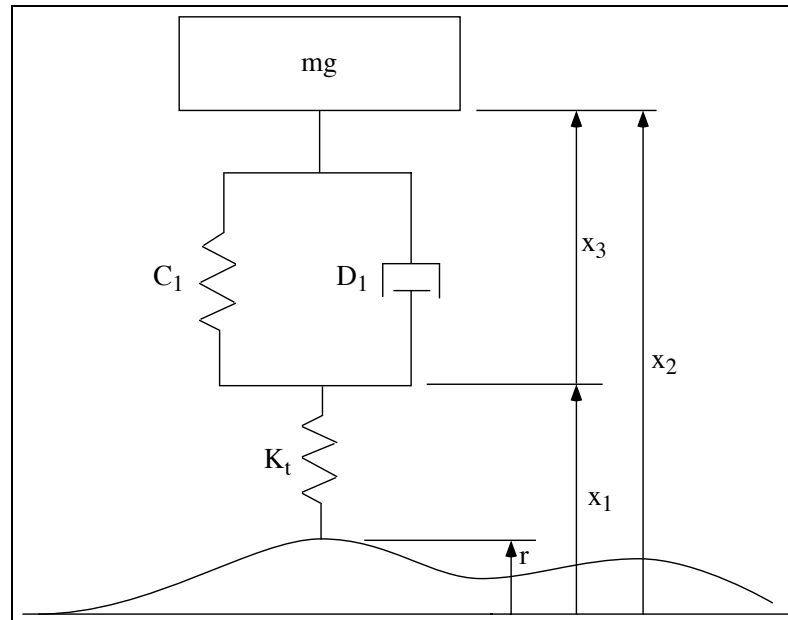


Figure 2.1: Simplified suspension and tire model.

express the dynamics of the suspension model using either suspension force or suspension length as states. Although both realizations are meant to model the same physical system, their reduced-order linearized dynamics can be very different. In the following sections,

two representations of the suspension model and their reduced-order linearized models are derived. In Section 2.2.1, suspension length is used as the suspension state. In Section 2.2.2, suspension force is used as the suspension state. Section 2.2.3 provides more discussion and a numerical example is given to illustrate the modelling difficulty.

### 2.2.1 Suspension Model With Suspension Length State

In this section, the suspension model uses suspension length as the state. The suspension force  $F_s$  acting on each wheel is given by

$$F_s = -C_1(x_3 - x_{30})[1 + C_2(x_3 - x_{30})^4] - D_1\dot{x}_3 + mg \quad (2.1)$$

where  $x_{30}$  is the length of the suspension system when a nominal load  $mg$  is applied. Compare this with Equation 2.3 of (Douglas et al. 1996).

The force  $F_t$  transmitted to the suspension by the tire spring is given by

$$F_t = -K_t(x_2 - x_3 - r - x_{10}) \quad (2.2)$$

where  $K_t$  is the tire spring stiffness and  $x_{10}$  is the nominal tire radius. Since the tire is massless, the tire spring force is equal to the suspension force.

$$F_t = F_s \quad (2.3)$$

Put (2.1) and (2.2) into (2.3),

$$\dot{x}_3 = \frac{1}{D_1}[-(K_t + C_1)x_3 + K_t x_2 - C_1 C_2 (x_3 - x_{30})^5 - K_t r + (mg + C_1 x_{30} - K_t x_{10})] \quad (2.4)$$

An equation of motion for the chassis given by

$$m\ddot{x}_2 = K_t(-x_2 + x_3 + r + x_{10}) \quad (2.5)$$

provides another relation between  $x_2$  and  $x_3$ .

The dynamics (2.4, 2.5) after a linearization become

$$\frac{d}{dt} \begin{bmatrix} x_2 \\ \dot{x}_2 \\ x_3 \end{bmatrix} = \begin{bmatrix} 0 & 1 & 0 \\ -\frac{K_t}{D_1} & 0 & \frac{K_t}{D_1} \\ \frac{K_t}{D_1} & 0 & -\frac{K_t + C_1}{D_1} \end{bmatrix} \begin{bmatrix} x_2 \\ \dot{x}_2 \\ x_3 \end{bmatrix} + \begin{bmatrix} 0 \\ \frac{K_t}{D_1} \\ -\frac{K_t}{D_1} \end{bmatrix} r$$



with the characteristic equation

$$s^3 + \frac{K_t + C_1}{D_1} s^2 + \frac{K_t}{m} s + \frac{K_t C_1}{m D_1} = 0 \quad (2.6)$$

The linearized dynamics order is reduced by noting that the suspension length state  $x_3$  is fast. See the example in Section 2.2.3. Let  $\dot{x}_3 = 0$  and algebraically eliminate  $x_3$  as a linear combination of  $x_2$  and  $\dot{x}_2$ .

$$\frac{d}{dt} \begin{bmatrix} x_2 \\ \dot{x}_2 \end{bmatrix} = \begin{bmatrix} 0 & 1 \\ -\frac{K_t C_1}{m(K_t + C_1)} & 0 \end{bmatrix} \begin{bmatrix} x_2 \\ \dot{x}_2 \end{bmatrix} + \begin{bmatrix} 0 \\ \frac{K_t C_1}{m(K_t + C_1)} \end{bmatrix} r$$

The reduced-order dynamics characteristic equation is

$$s^2 + \frac{K_t C_1}{m(K_t + C_1)} = 0 \quad (2.7)$$

Clearly, the reduced-order dynamics (2.7) are very different from the full-order dynamics (2.6) since the reduced-order dynamics exhibit no damping. The eigenvalues of the full and reduced-order linearized models are evaluated in the example of Section 2.2.3.

### 2.2.2 Suspension Model With Suspension Force State

In this section, the suspension model uses suspension force as the state. Start with (2.1, 2.2, 2.3) of the last section

$$F_s = -C_1(x_2 - x_1 - x_{30})[1 + C_2(x_2 - x_1 - x_{30})^4] - D_1(\dot{x}_2 - \dot{x}_1) + mg \quad (2.8a)$$

$$F_t = -K_t(x_1 - r - x_{10}) \quad (2.8b)$$

$$F_t = F_s \quad (2.8c)$$

The tire spring force  $F_t$  is eliminated by rearranging (2.5) to get

$$x_1 = r + x_{10} - \frac{F_t}{K_t} \quad (2.9a)$$

$$\dot{x}_1 = \dot{r} - \frac{\dot{F}_t}{K_t} \quad (2.9b)$$

and then combining (2.8a), (2.8c) and (2.9) as

$$\dot{F} = \frac{K_t}{D_1} \left\{ -F + mg - C_1(x_2 - r - x_{10} - x_{30} + \frac{F}{K_t}) \right. \\ \left. [1 + C_2(x_2 - r - x_{10} - x_{30} + \frac{F}{K_t})^4] - D_1(\dot{x}_2 - \dot{r}) \right\}$$

where  $F \triangleq F_s$ . An equation of motion for the chassis is given by combining (2.5) with (2.8b) and (2.8c)

$$m\ddot{x}_2 = F$$

The linearized model is

$$\frac{d}{dt} \begin{bmatrix} x_2 \\ \dot{x}_2 \\ F \end{bmatrix} = \begin{bmatrix} 0 & 1 & 0 \\ 0 & 0 & \frac{1}{m} \\ -\frac{K_t C_1}{D_1} & -K_t & -\frac{K_t + C_1}{D_1} \end{bmatrix} \begin{bmatrix} x_2 \\ \dot{x}_2 \\ F \end{bmatrix} + \begin{bmatrix} 0 & 0 \\ 0 & 0 \\ \frac{K_t C_1}{D_1} & K_t \end{bmatrix} \begin{bmatrix} r \\ \dot{r} \end{bmatrix}$$

with the characteristic equation

$$s^3 + \frac{K_t + C_1}{D_1} s^2 + \frac{K_t}{m} s + \frac{K_t C_1}{m D_1} = 0 \quad (2.10)$$

which is the same as (2.6) as expected.

Again, since the suspension force state  $F$  is fast, the reduced-order linearized model is derived by letting  $\dot{F} = 0$  and algebraically eliminating  $F$  as a linear combination of  $x_2$  and  $\dot{x}_2$ .

$$\frac{d}{dt} \begin{bmatrix} x_2 \\ \dot{x}_2 \end{bmatrix} = \begin{bmatrix} 0 & 1 \\ -\frac{K_t C_1}{m(K_t + C_1)} & -\frac{K_t D_1}{m(K_t + C_1)} \end{bmatrix} \begin{bmatrix} x_2 \\ \dot{x}_2 \end{bmatrix} + \begin{bmatrix} 0 & 0 \\ \frac{K_t C_1}{m(K_t + C_1)} & \frac{K_t D_1}{m(K_t + C_1)} \end{bmatrix} \begin{bmatrix} r \\ \dot{r} \end{bmatrix}$$

The reduced-order dynamics characteristic equation is

$$s^2 + \frac{K_t D_1}{m(K_t + C_1)} s + \frac{K_t C_1}{m(K_t + C_1)} = 0 \quad (2.11)$$

This reduced-order model includes a damping term and is probably a more realistic model than the reduced-order model of Section 2.2.1. However, note that this model regards road displacement  $r$  and road displacement rate  $\dot{r}$  as two independent inputs. In the physical system being modelled, they are not independent. The eigenvalues of this model are also evaluated in Section 2.2.3.

### 2.2.3 Example

Here is a numerical example of a suspension model. The parameters are obtained from the vehicle simulation code from U.C. Berkeley.

$$\begin{aligned}
 m &= 393.25 \text{ kg} && \text{Mass of a quarter car.} \\
 K_t &= 190632 \frac{\text{N}}{\text{m}} && \text{Tire spring constant.} \\
 C_1 &= 17000 \frac{\text{N}}{\text{m}} && \text{Suspension spring constant.} \\
 D_1 &= 1500 \frac{\text{N} \cdot \text{s}}{\text{m}} && \text{Suspension damper constant.}
 \end{aligned}$$

The eigenvalues of both full-order models in Section 2.2.1 and 2.2.2 are the same:  $-135.13, -1.64 \pm 6.16i$ . The eigenvalues of the reduced-order model in Section 2.2.1 are  $\pm 6.30i$  and the eigenvalues of the reduced-order model in Section 2.2.2 are  $-1.75 \pm 6.05i$ . The light damping of the force-state model of Section 2.2.2 is more realistic so this model is considered to be a better representation of the suspension dynamics.

**Remark 1.** If the model reduction is done by balanced realization and truncation, the length-state and force-state realizations should have similar reduced-order linear models. Balanced realization and truncation, discussed in detail in (Douglas et al. 1996), truncates the least observable and controllable modes as determined by inspection of the observability and controllability Grammians. By this method, the truncated modes are not necessarily the fast modes so that the eigenvalues of the reduced-order model might be very different from those of the full-order model. Further, when fast modes are truncated, the simple state truncation with steady-state correction method illustrated in Sections 2.2.1 and 2.2.2 produces results that are dependent on the state basis. Regarding a balanced realization as just another basis, it is possible that for some problems, a balanced realization does not provide a best reduced-order model. Best is problem dependent but is generally determined by comparing the full and reduced-order frequency responses and eigenstructures. ◀

### 2.3 Manifold Temperature Model

In the engine model the manifold temperature is taken to be a constant. If a manifold temperature sensor is to be monitored for a fault, two sensor models are possible. One model has the manifold temperature as an engine state and appends an integrator to the engine dynamics. Another model considers the manifold temperature as a measured exogenous input.

Since manifold temperature changes are on a much longer time scale than the engine dynamics, it is a natural choice to model the manifold temperature as a constant. With a constant manifold temperature as an engine state, an integrator is appended to the engine dynamics.

$$\begin{aligned} \begin{bmatrix} \dot{x} \\ \dot{x}_{T_m} \end{bmatrix} &= \begin{bmatrix} A & B_{T_m} \\ 0 & 0 \end{bmatrix} \begin{bmatrix} x \\ x_{T_m} \end{bmatrix} + \begin{bmatrix} B \\ 0 \end{bmatrix} u \\ y &= \begin{bmatrix} C & 0 \\ 0 & 1 \end{bmatrix} \begin{bmatrix} x \\ x_{T_m} \end{bmatrix} \end{aligned}$$

where  $x_{T_m}$  is the manifold temperature state and  $x$  are the rest of the states. A problem with this model is that the observability Grammian is ill-defined because the eigenvalue at the origin is associated with a measured state, the temperature  $x_{T_m}$ .

An alternate model has the temperature as a known, that is measured, input to the engine.

$$\begin{aligned} \dot{x} &= Ax + Bu + B_{T_m} \omega_{T_m} \\ y_x &= Cx \\ y_\omega &= \omega_{T_m} \end{aligned}$$

This approach avoids the observability Grammian problem and seems more reasonable in that the manifold temperature is an environmental factor which cannot be controlled.

## Fault Detection By Analytic Redundancy

---

ANALYTIC REDUNDANCY is an approach to health monitoring that compares dissimilar instruments using a detailed system model. The approach is to find dynamic or algebraic relationships between sensors and actuators. That is, information provided by a monitored sensor is, in some form, also provided by other sensors or, through the dynamics, by actuator commands. In automated vehicles, these requirements preclude monitoring nonredundant sensors such as obstacle detection or lane position sensors. The information provided by a radar or infrared sensor designed to detect objects in the vehicle's path has no dynamic correlation with other sensors on the vehicle. A sensor that detects the vehicle's position in a lane is the only sensor that can provide this information. Actuators that do no observable action are also difficult to monitor. For example, the health of a power window actuator is easily monitored by the driver. But, unless specialized sensors are installed, no other part of the car is affected by the operation of this actuator and there is no analytic redundancy.

A range sensor is another example of a sensor for which a vehicle has no redundant information. In some configurations, range information is provided by several different

types of sensors, for example, radar and optical range sensors. In this type of design, the sensor measurements are fused at the vehicle regulation layer. So, for the purposes of vehicle control and fault detection, the range sensors are regarded as providing a single synthesized, and nonredundant, measurement.

Analytic dynamic redundancy requires a detailed model of the dynamic relationship between sensors and actuator commands. This information is encoded in a fault detection filter that detects and isolates faults by producing a static pattern in a linear observer residual. Most sensors and actuators associated with the vehicle longitudinal dynamics are monitored this way. Fault detection filter design is described in Section 3.1. Algebraic redundancy provides a simple algebraic parity equation that must be satisfied. For example, since the throttle actuator dynamics are very fast, the throttle actuator command minus the throttle actuator position is nominally zero. Parity equation design is described in 3.2. The fault detection and isolation system is summarized in Section 3.3.

### 3.1 Analytic Redundancy

Eleven sensors and two actuators are to be monitored. The sensors are the manifold air mass sensor  $y_{m_a}$ , engine speed sensor  $y_{\omega_e}$ , manifold temperature sensor  $y_{T_m}$ , manifold pressure sensor  $y_{p_m}$ , longitudinal velocity sensor  $y_{v_x}$  and accelerometer  $y_{a_x}$ , vertical accelerometer  $y_{a_z}$ , the sum of front wheel speed sensors  $y_{\bar{\omega}_f}$ , the sum of rear wheel speed sensors  $y_{\bar{\omega}_r}$ , throttle sensor  $y_{\alpha}$  and brake sensor  $y_{T_b}$ . The two actuators are the throttle  $u_{\alpha}$  and brake  $u_{T_b}$ . Three of the sensors  $y_{\alpha}$ ,  $y_{T_b}$  and  $y_{p_m}$ , are monitored with algebraically redundant information. Hence, eight sensors and two actuators are included in the fault detection filter design.

A very brief review of the fault detection filter is provided in Section 3.1.1. Section 3.1.2 describes the sensor and actuator fault models. Section 3.1.3 discusses several design considerations that are specific to the longitudinal vehicle dynamics health monitoring problem. Section 3.1.4 discusses how multiple faults are grouped among several filters. The fault detection filter designs are sensor and actuator fault groups described in Sections 3.1.5

and 3.1.6.

### 3.1.1 Beard-Jones Fault Detection Filter Background

A detailed review of fault detection filter design is provided in Appendix A of last year's report (Douglas et al. 1996). For a thorough background, several references are available, a few of which are (Douglas 1993), (White and Speyer 1987) and (Massoumnia 1986).

Consider a linear time-invariant system with  $q$  failure modes and no disturbances or sensor noise

$$\dot{x} = Ax + Bu + \sum_{i=1}^q F_i m_i \quad (3.1a)$$

$$y = Cx + Du \quad (3.1b)$$

The system variables  $x$ ,  $u$ ,  $y$  and the  $m_i$  belong to real vector spaces and the system maps  $A$ ,  $B$ ,  $C$ ,  $D$  and the  $F_i$  are of compatible dimensions. Assume that the input  $u$  and the output  $y$  both are known. The  $F_i$  are the failure signatures. They are known and fixed and model the directional characteristics of the faults. The  $m_i$  are the failure modes and model the unknown time-varying amplitude of faults. The  $m_i$  do not have to be scalar values.

A fault detection filter is a linear observer that, like any other linear observer, forms a residual process sensitive to unknown inputs. Consider a full-order observer with dynamics and residual

$$\dot{\hat{x}} = (A + LC)\hat{x} + Bu - Ly \quad (3.2a)$$

$$r = C\hat{x} + Du - y \quad (3.2b)$$

Form the state estimation error  $e = \hat{x} - x$  and the dynamics and residual are

$$\dot{e} = (A + LC)e - \sum_{i=1}^q F_i m_i$$

$$r = Ce$$

In steady-state, the residual is driven by the faults when they are present. If the system is  $(C, A)$  observable, and the observer dynamics are stable, then in steady-state and in the

absence of disturbances and modeling errors, the residual  $r$  is nonzero only if a fault has occurred, that is, if some  $m_i$  is nonzero. Furthermore, when a fault does occur, the residual is nonzero except in certain theoretically relevant but physically unrealistic situations. This means that any stable observer can detect the presence of a fault. Simply monitor the residual and when it is nonzero a fault has occurred.

In addition to detecting a fault, a fault detection filter provides information to determine which fault has occurred. An observer such as (3.2) becomes a fault detection filter when the observer gain  $L$  is chosen so that the residual has certain directional properties that immediately identify the fault. The gain is chosen to partition the residual space where each partition is uniquely associated with one of the design fault directions  $F_i$ . A fault is identified by projecting the residual onto each of the residual subspaces and then determining which projections are nonzero.

In a detection filter, the state estimation error in response to a fault in the direction  $F_i$  remains in a state subspace  $\mathcal{T}_i^*$ , an unobservability subspace or detection space. See Appendix A of last year's report (Douglas et al. 1996) for details. The ability to identify a fault, to distinguish one fault from another, requires, for an observable system, that the detection spaces be independent. Thus, the number of faults that can be detected and identified by a fault detection filter is limited by the size of the state space and the sizes of the detection spaces associated with each of the faults. If the problem considered has more faults than can be accommodated by one fault detection filter, then a bank of filters will have to be constructed.

For a fault  $F_i$ , the approach to finding the detection space  $\mathcal{T}_i^*$  is to find the minimal  $(C, A)$ -invariant subspace  $\mathcal{W}_i^*$  that contains  $F_i$  and then to find the invariant zero directions of the triple  $(C, A, F_i)$ , if any. With the invariant zero directions denoted by  $\mathcal{V}_i$ , the minimal unobservability subspace  $\mathcal{T}_i^*$  is given by

$$\mathcal{T}_i^* = \mathcal{W}_i^* + \mathcal{V}_i$$

Before the fault detection filter design (3.2) can begin, a system model with faults has to be found with the form (3.1). This is discussed in the next section.



### 3.1.2 Fault Modelling

This section describes sensor and actuator fault models used for fault detection filter design. Two classes of sensor fault are considered. One measures a linear combination of states. For the longitudinal vehicle dynamics these include  $y_{m_a}$ ,  $y_{\omega_e}$ ,  $y_{v_x}$ ,  $y_{a_x}$ ,  $y_{a_z}$ ,  $y_{\bar{\omega}_f}$  and  $y_{\bar{\omega}_r}$ . Another class of sensor fault is one that measures exogenous inputs. The manifold temperature sensor is the only sensor in this class.

The fault of a sensor which measures system states can be modelled as an additive term in the measurement equation

$$y = Cx + E_i\mu_i \quad (3.3)$$

where  $E_i$  is a column vector of zeros except for a one in the  $i^{\text{th}}$  position and where  $\mu_i$  is an arbitrary time-varying scalar. This is explained in last year's report (Douglas et al. 1996) but is included here for completeness. Since, for fault detection filter design, faults are expressed as additive terms to the system dynamics, a way must be found to convert the  $E_i$  sensor fault form of (3.3) to an equivalent  $F_i$  form as in (3.1). Let  $F_i$  satisfy

$$CF_i = E_i$$

and define a state estimation error  $e$  as

$$e = x - \hat{x} + F_i\mu_i$$

Using (3.2), the error dynamics are

$$\dot{e} = (A + LC)e + F_i\dot{\mu}_i - AF_i\mu_i \quad (3.4)$$

and a sensor fault  $E_i$  in (3.3) is equivalent to a two-dimensional fault  $F_i$

$$\dot{x} = Ax + Bu + F_i m_i \quad \text{with } F_i = [F_i^1, F_i^2]$$

where the directions  $F_i^1$  and  $F_i^2$  are given by

$$E_i = CF_i^1 \quad (3.5a)$$

$$F_i^2 = AF_i^1 \quad (3.5b)$$

An interpretation of the effect of a sensor fault on observer error dynamics follows from (3.4) where  $F_i^1$  is the sensor fault rate  $\dot{\mu}_i$  direction and  $F_i^2$  is the sensor fault magnitude  $\mu_i$  direction. This interpretation suggests a possible simplification when information about the spectral content of the sensor fault is available. If it is known that a sensor fault has persistent and significant high frequency components, such as in the case of a noisy sensor, the fault direction could be approximated by the  $F_i^1$  direction alone. Or, if it is known that a sensor fault has only low frequency components, such as in the case of a bias, the fault direction could be approximated by the  $F_i^2$  direction alone. For example, if a sensor were to develop a bias, a transient would be likely to appear in all fault directions but, in steady-state, only the residual associated with the faulty sensor should be nonzero.

A linear model partitioned to isolate first-order actuator dynamics can be expressed as

$$\begin{bmatrix} \dot{x} \\ \dot{x}_a \end{bmatrix} = \begin{bmatrix} A & B \\ 0 & -\omega \end{bmatrix} \begin{bmatrix} x \\ x_a \end{bmatrix} + \begin{bmatrix} 0 \\ \omega \end{bmatrix} u + B_\omega \omega$$

where  $x_a$  is a vector of actuator states and  $\omega$  is an exogenous input. Typically, exogenous inputs are dynamic disturbances such as road noise and wind gusts and are not known or measured. However, as described in Section 2.3, the manifold temperature is modelled as a dynamic input and is measured. A fault in this sensor is modelled as a direction given by the associated column of the  $B_\omega$  matrix.

A fault in a control input is also modeled as an additive term in the system dynamics. In the case of a fault appearing at the input of an actuator, that is the actuator command, the fault has the same direction as the associated column of the  $[0, \omega]^T$  matrix. A fault appearing at the output of an actuator, the actuator position, has the same direction as the associated column of the  $[B^T, 0]^T$  matrix. In the vehicle model, the actuator dynamics are relatively fast and, in an approximation made here, are removed from the system model. Thus, the control inputs are applied directly to the system through a column of the  $B$  matrix.

### 3.1.3 Special Design Considerations

Several design considerations arise that are specific to the longitudinal vehicle dynamics health monitoring problem. One problem is a conditioning problem that arises from the model order reduction done in Section 2.1. Another concerns the output separability of the modeled faults. A third problem concerns a reasonable expectation that a fault detection filter should produce a nonzero fault residual for as long as a modeled fault is present.

#### *Ill-conditioned fault direction*

For all sensor and throttle actuator faults described in Section 3.1.2, the detection or minimal unobservability subspaces are given by the fault directions themselves, that is,

$$\mathcal{T}_i^* = \mathcal{W}_i^* + \mathcal{V}_i = \text{Im } F_i$$

For example, for the brake actuator,  $\mathcal{T}_i^* = \text{Im } F_i$  because  $CF_{u_{T_b}} \neq 0$ , (Douglas et al. 1996). However,  $CF_{u_{T_b}} \neq 0$  only holds for the reduced, eighth-order model. For the full-order model,  $CF_{u_{T_b}} = 0$  so  $F_{u_{T_b}}$  should be considered as a very weakly observable direction. For fault detection filter design, the brake actuator unobservability subspace is taken to be the second-order space given by

$$\mathcal{T}_{u_{T_b}}^* = \text{Im} \left[ F_{u_{T_b}}, AF_{u_{T_b}} \right]$$

#### *Output separability*

The output separability design requirement states that the residuals produced by design faults be pairwise linearly independent. Faults that are not output separable generate co-linear residuals and cannot be isolated. Output separability of two faults  $F_i$  and  $F_j$  is determined by

$$CT_i^* \cap CT_j^* = 0 \tag{3.6}$$

which may be checked by the column independence of realizations for  $CT_i$  and  $CT_j$ .

Performing the check (3.6) reveals that two pairs of faults are not output separable. The throttle actuator  $u_\alpha$  and manifold air mass sensor  $y_{m_a}$  faults are not output separable and the manifold temperature sensor  $y_{T_m}$  and manifold air mass sensor  $y_{m_a}$  faults are not output separable. The problem is summarized as

$$\begin{aligned} \mathcal{T}_{u_\alpha}^* &= F_{u_\alpha} \\ \mathcal{T}_{y_{T_m}}^* &= F_{y_{T_m}} \\ \mathcal{T}_{y_{m_a}}^* &= [F_{y_{m_a}} \quad AF_{y_{m_a}}] \\ F_{u_\alpha} &= F_{y_{m_a}} \\ F_{y_{T_m}} &= AF_{y_{m_a}} \end{aligned}$$

First, consider the throttle actuator and manifold air mass sensor faults where  $CF_{u_\alpha} = CF_{y_{m_a}}$  indicates that they cannot be isolated. As explained in Section 3.1.2, the direction of the air mass sensor fault magnitude is  $AF_{y_{m_a}}$  while the direction of the fault rate is  $F_{y_{m_a}}$ . The throttle actuator and air mass sensor faults become output separable if only the sensor fault magnitude direction is used. This design decision could allow a noisy but zero mean sensor fault to remain undetected through the direction  $CAF_{y_{m_a}}$ . Also, since the throttle fault detection space is spanned by  $F_{u_\alpha} = F_{y_{m_a}}$ , an air mass sensor fault rate will stimulate the throttle fault residual. However, a throttle actuator fault could never stimulate the air mass sensor fault residual. In summary, as long as the air mass sensor fault spectral components are low frequency, the throttle actuator and manifold air mass sensor faults should be detectable and isolatable.

Next, consider the manifold temperature and air mass sensor faults where  $CF_{y_{T_m}} = CAF_{y_{m_a}}$  indicates that they cannot be isolated. Since  $AF_{y_{m_a}}$  represents the fault magnitude direction, this direction can not be dropped from the detection space. One remedy is to design a second fault detection filter that does not take the manifold air mass as a measurement. Such a filter will be unaffected by air mass sensor faults but will respond to manifold temperature sensor faults. A problem with this fix is that the throttle actuator and temperature sensor faults are not output separable without an air mass sensor measurement.

Responses of the two filter designs are summarized in Figure 3.1. Each row represents a bias (hard) fault in either the throttle actuator, the air mass sensor or the temperature sensor. The columns are the residual responses to the given fault conditions. The first column is the response of the throttle actuator fault residual of the first filter. The second column is the response of the air mass sensor and temperature sensor fault residuals also from the first filter. The third column is the response of the throttle actuator and temperature sensor fault residuals of the second filter.

Figure 3.1 shows that neither filter alone can detect and isolate the three faults: the throttle actuator, the air mass sensor and the temperature sensor. Taken together, the two filters produce a pattern unique to each fault so that the faults may be isolated. However, the picture is not yet complete. A problem with the second fault detection filter is described in the next section.

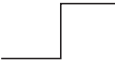

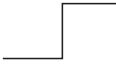

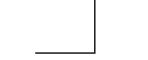


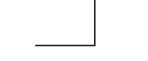

| Residual<br>Fault       | Detection Filter #1   |  | Detection<br>Filter #2  |
|-------------------------|---|--|---|
|                         | Throttle<br>Actuator  | Manifold Air Mass<br>and Temperature   |   |
| Throttle<br>Actuator    |  |  |  |
| Manifold<br>Air Mass    |  |  |  |
| Manifold<br>Temperature |  |  |  |

Figure 3.1: Fault Signatures.

### *Zero steady-state fault residual*

It is a reasonable expectation that a fault detection filter should produce a nonzero fault residual for as long as a modeled fault is present. A necessary and sufficient condition is given in the following theorem.

**Theorem 3.1.** A necessary and sufficient condition for a fault detection filter residual to hold a non-zero steady-state value in response to a bias fault is  $CA^{-1}F \neq 0$ , that is,

$$C(sI - A - LC)^{-1}F|_{s=0} = 0 \quad \Leftrightarrow \quad CA^{-1}F = 0$$

**Proof.** Let  $\bar{F} \triangleq (A + LC)^{-1}F$ . ( $\Rightarrow$ )

$$F = (A + LC)\bar{F} = A\bar{F} \quad \text{because } C\bar{F} = C(A + LC)^{-1}F = 0.$$

$$\Rightarrow \bar{F} = A^{-1}F$$

$$\Rightarrow CA^{-1}F = C\bar{F} = 0$$

( $\Leftarrow$ )

$$A\bar{F} + LC\bar{F} = F$$

$$\Rightarrow \bar{F} = A^{-1}F \quad \text{because } CA^{-1}F = 0 \text{ and } (A + LC) \text{ is unique.}$$

$$\Rightarrow C(A + LC)^{-1}F = C\bar{F} = CA^{-1}F = 0$$

Since  $CA^{-1}F_{y_{T_m}} = 0$ , the second fault detection filter will not see the temperature sensor faults in the steady state. When a temperature bias fault occurs, the residual responds with only a transient. Figure 3.1 is corrected in Figure 3.2 to illustrate the transitory response. Once again, the fault patterns for the three faults are not unique, at least not in steady-state.

Since a second fault detection filter no longer fixes the output separability problem, another fix is needed. An algebraic relation between the manifold pressure and manifold air mass is useful

$$\text{manifold pressure} - 19.9635 * \text{manifold air mass} = 0 \quad (3.7)$$

This convenient relation arises from the perfect gas law. The magic number 19.9635 includes the gas constant, a nominal temperature and the manifold volume. Equation (3.7) is a










| Residual<br>Fault    | Detection Filter #1   |  | Detection Filter #2   |
|----------------------|---|--|---|
|                      | Throttle Actuator   | Manifold Air Mass and Temperature  |   |
| Throttle Actuator    |  |  |  |
| Manifold Air Mass    |  |  |  |
| Manifold Temperature |  |  |  |

Figure 3.2: Fault Signatures.

parity equation that is satisfied when the manifold pressure and manifold air mass sensors are working and is not satisfied when either sensor has failed. The parity equation by itself cannot isolate a fault.

By combining the parity equation (3.7) with the first fault detection filter of the last section, a residual pattern unique to each fault is formed and the faults may be isolated. The faults are the throttle actuator, the air mass sensor, the temperature sensor and the manifold pressure sensor. The residual patterns are summarized in Figure 3.3 Each row represents a bias (hard) fault in either the throttle actuator, the air mass sensor, the temperature sensor or the manifold pressure sensor. The columns are the residual responses to the given fault conditions. The first column is the response of the throttle actuator fault residual of the first filter. The second column is the response of the air mass sensor and temperature sensor fault residuals also from the first filter. The third column is the response of the parity equation for the manifold air mass and pressure sensors. The parity equation is discussed further in Section 3.2.

### 3.1.4 Fault Assignment to Multiple Fault Detection Filters

The ability to identify a fault, to distinguish one fault from another, requires for an observable system that the detection spaces be independent. Therefore, the number of

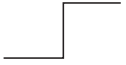











| Residual<br>Fault       | Detection Filter  |   | Parity<br>Equation   |
|-------------------------|---|---|--|
|                         | Throttle<br>Actuator  | Manifold Air Mass<br>And Temperature  |  |
| Throttle<br>Actuator    |  |  |  |
| Manifold<br>Air Mass    |  |  |  |
| Manifold<br>Temperature |  |  |  |
| Manifold<br>Pressure    |  |  |  |

Figure 3.3: Fault Signatures.

faults that can be detected and identified by a fault detection filter is limited by the size of the state space and the sizes of the detection spaces associated with each of the faults. If the problem considered has more faults than can be accommodated by one fault detection filter, then a bank of filters will have to be constructed. The health monitoring system described in this section for a vehicle going straight, considers nine system faults: seven sensor faults and two actuator faults. Since the reduced-order longitudinal model has eight states and seven measurements, clearly more than one fault detection filter is needed. The dimension of the throttle actuator, the manifold air mass sensor and the manifold temperature sensor detection spaces is one. The dimension of the brake actuator and the rest of the sensor faults is two. Therefore, for this problem at least three filters are needed.

One consideration in grouping the faults among the fault detection filters is to group faults which are robust to system nonlinearities. Note that an actuator fault changes the vehicle operating point possibly introducing nonlinear effects into all measurements. The nonlinear effect is small if the residual response is small compared to that for some nominal fault. Also, sensor faults that are open-loop are easily isolated since they do not stimulate any dynamics. One approach to fault grouping is to always group actuator and sensor faults



with different fault detection filters.

Usually an attempt is made to group as many faults as possible in each filter. When full-order filters are used, this approach minimizes the number of filters needed. When reduced-order filters are used, this approach minimizes the order of each complementary space and, therefore, the order of each reduced-order filter. Note that each fault included in a fault detection filter design imposes more constraints on the filter eigenvectors. Sometimes, the objective of obtaining well-conditioned filter eigenvectors imposes a tradeoff between robustness and the reduced-order filter size.

With all the considerations above in mind, now we should decide how many fault detection filters are needed and which faults should go together. Robustness to nonlinearities requires all the actuator faults to be in the same filter. The output separability consideration of Section 3.1.3 requires the throttle actuator and manifold air mass sensor fault to be in the same filter. Thus, one fault detection filter has the throttle actuator  $u_\alpha$ , brake actuator  $u_{T_b}$  and manifold air mass sensor  $y_{m_a}$ . Note that this filter is also sensitive to faults in the manifold temperature sensor  $y_{T_m}$  since manifold temperature and manifold air mass sensor faults are not output separable.

The six remaining sensor faults,  $y_{\omega_e}$ ,  $y_{v_x}$ ,  $y_{a_x}$ ,  $y_{a_z}$ ,  $y_{\bar{\omega}_f}$  and  $y_{\bar{\omega}_r}$  are assigned to two more fault detection filters. Each filter has three faults. There are ten different combinations for these two filters and they are all non-mutually detectable which means the invariant zeros arising from the fault combinations will be the eigenvalues of the filters, that is, some poles of the filters cannot be assigned. In six of these cases, the invariant zeros, hence the fixed poles, are in the right-half plane resulting in an unstable fault detection filter. The remaining four configurations are stable. Each stable case has been designed and tested. The most robust combination is to put  $y_{\omega_e}$ ,  $y_{a_x}$  and  $y_{\bar{\omega}_f}$  into the second filter and put  $y_{v_x}$ ,  $y_{a_z}$  and  $y_{\bar{\omega}_r}$  into the third filter. Here, *most robust* is taken to mean the filter with left eigenvectors that are least ill-conditioned. This hedges against eigenstructure sensitivity to small variations in system parameters. The three fault detection filters are

Fault detection filter 1.

$u_\alpha$  : Throttle actuator.

$u_{T_b}$  : Brake actuator.

$y_{m_a}$  : Manifold air mass sensor.

$y_{T_m}$  : Manifold temperature sensor.

Fault detection filter 2.

$y_{\omega_e}$  : Engine speed sensor.

$y_{a_x}$  : Longitudinal accelerometer.

$y_{\bar{\omega}_f}$  : Sum of front wheel speed sensors.

Fault detection filter 3.

$y_{v_x}$  : Longitudinal velocity sensor.

$y_{a_z}$  : Vertical accelerometer.

$y_{\bar{\omega}_r}$  : Sum of rear wheel speed sensors.

### 3.1.5 Fault Detection Filter Design For Sensors

In this and the following sections, Beard-Jones fault detection filters have been designed using eigenstructure assignment while ensuring that the eigenvectors are not ill-conditioned. The essential feature of a fault detection filter is the detection space structure embedded in the filter dynamics. A left eigenvector assignment design algorithm explicitly places eigenvectors to span these subspaces. An eigenvector assignment design algorithm also has to balance the objective of having well-conditioned eigenvectors for robustness against the objective of each fault being highly input observable for fault detection performance. System disturbances, sensor noise and system parameter variations are not considered in the fault detection filter designs described in this report. Note that they are considered in performance evaluation. For such a benign environment, the filter designs are based on

spectral considerations only; there is little else that can be used to distinguish a good design from a bad design.

Since the calculations are somewhat long and they are the similar for each detection filter, the calculation details are given for only the first and third fault detection filters. In this section, the fault detection filter is designed for the third fault group which has the longitudinal velocity sensor  $y_{v_x}$ , the vertical accelerometer  $y_{a_z}$  and the sum of rear wheel speed sensors  $y_{\bar{\omega}_r}$ . In next section, a filter is designed for the first fault group which has the throttle actuator  $u_\alpha$ , the brake actuator  $u_{T_b}$  and the manifold air mass sensor  $y_{m_a}$ . Note once again that the manifold air mass sensor  $y_{m_a}$  is not output separable with respect to the manifold temperature sensor  $y_{T_m}$ .

The eight state reduced-order longitudinal model derived in Section 2.1 is used. The dimension of each detection space was found in Section 3.1.4 as

$$\begin{aligned}\nu_{y_{v_x}} &= \dim \mathcal{T}_{y_{v_x}}^* = 2 \\ \nu_{y_{a_z}} &= \dim \mathcal{T}_{y_{a_z}}^* = 2 \\ \nu_{y_{\bar{\omega}_r}} &= \dim \mathcal{T}_{y_{\bar{\omega}_r}}^* = 2\end{aligned}$$

The dimension of the fault detection filter complementary space  $\mathcal{T}_0$  is also needed. The complementary space is any subspace independent of the detection spaces that completes the state-space.

$$\mathcal{X} = \mathcal{T}_{y_{v_x}}^* \oplus \mathcal{T}_{y_{a_z}}^* \oplus \mathcal{T}_{y_{\bar{\omega}_r}}^* \oplus \mathcal{T}_0$$

Thus the dimension of  $\mathcal{T}_0$  is two

$$\begin{aligned}\nu_0 &= n - \nu_{y_{v_x}} - \nu_{y_{a_z}} - \nu_{y_{\bar{\omega}_r}} \\ &= 8 - 2 - 2 - 2 \\ &= 2\end{aligned}$$

Next define the complementary faults sets. There are three faults  $F_{y_{v_x}}$ ,  $F_{y_{a_z}}$  and  $F_{y_{\bar{\omega}_r}}$

so there are four complementary fault sets which are:

$$\hat{F}_{y_{v_x}} = [F_{y_{a_z}}, F_{y_{\bar{\omega}_r}}] \quad (3.8a)$$

$$\hat{F}_{y_{a_z}} = [F_{y_{v_x}}, F_{y_{\bar{\omega}_r}}] \quad (3.8b)$$

$$\hat{F}_{y_{\bar{\omega}_r}} = [F_{y_{v_x}}, F_{y_{a_z}}] \quad (3.8c)$$

$$\hat{F}_0 = [F_{y_{v_x}}, F_{y_{a_z}}, F_{y_{\bar{\omega}_r}}] \quad (3.8d)$$

Now choose the filter closed-loop eigenvalues. As discussed in Section 3.1.4, these three faults are not mutually detectable. Therefore the invariant zero  $-14.52$  has to be one of the eigenvalues of the complementary subspace. Since the system model includes no sensor noise, no disturbances and no parameter variations, there is little basis for preferring one set of detection filter closed-loop eigenvalues over another. The poles are chosen here to give a reasonable response time but are not unrealistically fast. The assigned eigenvalues are

$$\Lambda_{y_{v_x}} = \{-3, -4\}$$

$$\Lambda_{y_{a_z}} = \{-3, -4\}$$

$$\Lambda_{y_{\bar{\omega}_r}} = \{-3, -4\}$$

$$\Lambda_0 = \{-3, -14.52\}$$

The next step is to find the closed-loop fault detection filter left eigenvectors. For each eigenvalue  $\lambda_{i_j} \in \Lambda_i$ , the left eigenvectors  $v_{i_j}$  generally are not unique and must be chosen from a subspace as  $v_{i_j} \in V_{i_j}$  where  $V_{i_j}$  and another space  $W_{i_j}$  are found by solving

$$\begin{bmatrix} A^T - \lambda_{i_j} I & C^T \\ \hat{F}_i^T & 0 \end{bmatrix} \begin{bmatrix} V_{i_j} \\ W_{i_j} \end{bmatrix} = \begin{bmatrix} 0 \\ 0 \end{bmatrix} \quad (3.9)$$

There are eight  $V_{i_j}$  associated with eight eigenvalues. To help desensitize the fault detection filter to parameter variations, the left eigenvectors are chosen from  $v_{i_j} \in V_{i_j}$  as the set with the greatest degree of linear independence. The degree of linear independence is indicated by the smallest singular value of the matrix formed by the left eigenvectors. Upper bounds

on the singular values of the left eigenvectors are given by the singular values of

$$V = [V_{0_1}, V_{0_2}, V_{y_{v_{x1}}}, V_{y_{v_{x2}}}, V_{y_{a_{z1}}}, V_{y_{a_{z2}}}, V_{y_{\bar{\omega}_{r1}}}, V_{y_{\bar{\omega}_{r2}}}]$$

These singular values are

$$\sigma(V) = \{2.83, 2.50, 1.69, 1.41, 1.32, 0.333, 0.080, 0.0088\} \quad (3.10)$$

If the left eigenvector singular value upper bounds were small, then all possible combinations of detection filter left eigenvectors would be ill-conditioned and the filter eigenstructure would be sensitive to small parameter variations. Since (3.10) indicates that the upper bounds are not small, continue by looking for a set of fault detection filter left eigenvectors that are reasonably well-conditioned. For this case, one possible set of left eigenvectors from the set  $V$  nearly meets the upper bound and should be well-conditioned. The singular values of this set of left eigenvectors are

$$\sigma(\tilde{V}) = \{1.95, 1.12, 1.00, 1.00, 0.92, 0.285, 0.063, 0.00691\}$$

Since the difference between the largest and the smallest singular values is only three orders of magnitude, the detection filter gain will be reasonably small and the filter eigenstructure should not be sensitive to small parameter variations.

The fault detection filter gain  $L$  is found by solving

$$\tilde{V}^T L = \tilde{W}^T \quad (3.11)$$

where  $\tilde{V}$  is the matrix of left eigenvectors as found above, and  $\tilde{W}$  is a matrix of vectors  $w_{i_j}$

$$\begin{bmatrix} A^T - \lambda_{i_j} I & C^T \\ \hat{F}_i^T & 0 \end{bmatrix} \begin{bmatrix} v_{i_j} \\ w_{i_j} \end{bmatrix} = \begin{bmatrix} 0 \\ 0 \end{bmatrix}$$

If the left eigenvector  $v_{i_j}$  is a linear combination of the columns of  $V_{i_j}$ ,  $w_{i_j}$  is the same linear combination of the columns of  $W_{i_j}$  where  $V_{i_j}$  and  $W_{i_j}$  are from (3.9).

To complete the detection filter design, output projection matrices  $\hat{H}_{y_{v_x}}$ ,  $\hat{H}_{y_{a_z}}$  and  $\hat{H}_{y_{\bar{\omega}_r}}$  are needed to project the residual along the respective output subspaces  $C\hat{T}_{y_{v_x}}^*$ ,  $C\hat{T}_{y_{a_z}}^*$  and

$C\hat{T}_{y\bar{\omega}_r}^*$ . What this means is that, for example,  $\hat{T}_{y_{v_x}}^*$  becomes the unobservable subspace of the pair  $(\hat{H}_{y_{v_x}}C, A + LC)$ . Remember that by the definition of the complementary faults (3.8), faults  $F_{y_{a_z}}$  and  $F_{y_{\bar{\omega}_r}}$  lie in  $\hat{T}_{y_{v_x}}^*$  and fault  $F_{y_{v_x}}$  does not. The effect is that the projected residual is driven by fault  $F_{y_{v_x}}$  and only fault  $F_{y_{v_x}}$ .

A projection  $\hat{H}_i$  is computed by first finding a basis for the range space of  $C\hat{T}_i^*$  where again,  $\hat{T}_i^*$  is any basis for the detection space  $\hat{T}_i^*$ . This is done by finding the left singular vectors of  $C\hat{T}_i^*$ . Denote this basis for now as  $h_i$ . Then  $\hat{H}_i$  is given by

$$\hat{H}_i = I - h_i h_i^T$$

In summary, a fault detection filter for the system with sensor faults  $E_{y_{v_x}}$ ,  $E_{y_{a_z}}$  and  $E_{y_{\bar{\omega}_r}}$

$$\begin{aligned}\dot{x} &= Ax + Bu + B_{T_m}\omega_{T_m} \\ y &= Cx + Du + E_{y_{v_x}}\mu_{y_{v_x}} + E_{y_{a_z}}\mu_{y_{a_z}} + E_{y_{\bar{\omega}_r}}\mu_{y_{\bar{\omega}_r}}\end{aligned}$$

is equivalent to a fault detection filter for the system with faults  $F_{y_{v_x}}$ ,  $F_{y_{a_z}}$  and  $F_{y_{\bar{\omega}_r}}$

$$\begin{aligned}\dot{x} &= Ax + Bu + B_{T_m}\omega_{T_m} + F_{y_{v_x}}m_{y_{v_x}} + F_{y_{a_z}}m_{y_{a_z}} + F_{y_{\bar{\omega}_r}}m_{y_{\bar{\omega}_r}} \\ y &= Cx + Du\end{aligned}$$

and has the form

$$\begin{aligned}\dot{\hat{x}} &= (A + LC)\hat{x} + (B + LD)u + B_{T_m}y_{T_m} - Ly \\ z_{y_{v_x}} &= \hat{H}_{y_{v_x}}(C\hat{x} + Du - y) \\ z_{y_{a_z}} &= \hat{H}_{y_{a_z}}(C\hat{x} + Du - y) \\ z_{y_{\bar{\omega}_r}} &= \hat{H}_{y_{\bar{\omega}_r}}(C\hat{x} + Du - y)\end{aligned}$$

where  $L$ ,  $\hat{H}_{y_{v_x}}$ ,  $\hat{H}_{y_{a_z}}$  and  $\hat{H}_{y_{\bar{\omega}_r}}$  are shown in Appendix A.

A fault detection filter design for the second fault group is carried out in the similar way and is not shown here. However, the filter gain  $L$  and projections  $\hat{H}_{y_{\omega_e}}$ ,  $\hat{H}_{y_{a_x}}$  and  $\hat{H}_{y_{\bar{\omega}_f}}$  are shown in Appendix A.

### 3.1.6 Fault Detection Filter Design For Actuators

In next section, a fault detection filter is designed for the first fault group which has the throttle actuator  $u_\alpha$ , the brake actuator  $u_{T_b}$  and the manifold air mass sensor  $y_{m_a}$ . Note once again that the manifold air mass sensor  $y_{m_a}$  is not output separable with respect to the manifold temperature sensor  $y_{T_m}$ .

The design procedure is similar to the previous section but does have a twist. As discussed in Section 3.1.3, a reduced-order manifold air mass sensor fault is used to achieve output separability with the throttle actuator fault. Also manifold air mass and manifold temperature sensor faults cannot be isolated.

The dimension of each detection space was found in Section 3.1.4 as

$$\nu_{u_\alpha} = \dim \mathcal{T}_{u_\alpha}^* = 1$$

$$\nu_{u_{T_b}} = \dim \mathcal{T}_{u_{T_b}}^* = 2$$

$$\nu_{y_{m_a}} = \dim \mathcal{T}_{y_{m_a}}^* = 1$$

and the dimension of the fault detection filter complementary space  $\mathcal{T}_0$  where

$$\mathcal{X} = \mathcal{T}_{u_\alpha}^* \oplus \mathcal{T}_{u_{T_b}}^* \oplus \mathcal{T}_{y_{m_a}}^* \oplus \mathcal{T}_0$$

is four

$$\begin{aligned} \nu_0 &= n - \nu_{u_\alpha} - \nu_{u_{T_b}} - \nu_{y_{m_a}} \\ &= 8 - 1 - 2 - 1 \\ &= 4 \end{aligned}$$

Next define the complementary faults sets. There are three faults  $F_{u_\alpha}$ ,  $F_{u_{T_b}}$  and  $F_{y_{m_a}}$  so there are four complementary fault sets which are:

$$\hat{F}_{u_\alpha} = [F_{u_{T_b}}, F_{y_{m_a}}] \quad (3.12a)$$

$$\hat{F}_{u_{T_b}} = [F_{u_\alpha}, F_{y_{m_a}}] \quad (3.12b)$$

$$\hat{F}_{y_{m_a}} = [F_{u_\alpha}, F_{u_{T_b}}] \quad (3.12c)$$

$$\hat{F}_0 = [F_{u_\alpha}, F_{u_{T_b}}, F_{y_{m_a}}] \quad (3.12d)$$

Now choose the fault detection filter closed-loop eigenvalues. Since these three faults are mutually detectable, all eigenvalues are freely assignable.

$$\begin{aligned}\Lambda_{u_\alpha} &= \{-3\} \\ \Lambda_{u_{T_b}} &= \{-3, -4\} \\ \Lambda_{y_{m_a}} &= \{-3\} \\ \Lambda_0 &= \{-3, -4, -5, -6\}\end{aligned}$$

The next step is to find the closed-loop fault detection filter left eigenvectors. The left eigenvectors  $v_{i_j}$  for each eigenvalue  $\lambda_{i_j} \in \Lambda_i$  generally are not unique and must be chosen from a subspace as  $v_{i_j} \in V_{i_j}$  where  $V_{i_j}$  is found by solving

$$\begin{bmatrix} A^T - \lambda_{i_j} I & C^T \\ \hat{F}_i^T & 0 \end{bmatrix} \begin{bmatrix} V_{i_j} \\ W_{i_j} \end{bmatrix} = \begin{bmatrix} 0 \\ 0 \end{bmatrix} \quad (3.13)$$

There are eight  $V_{i_j}$  associated with eight eigenvalues. Upper bounds on the singular values of the left eigenvectors are given by the singular values of

$$V = [V_{0_1}, V_{0_2}, V_{0_3}, V_{0_4}, V_{u_\alpha}, V_{u_{T_{b1}}}, V_{u_{T_{b2}}}, V_{y_{m_a}}]$$

These singular values are

$$\sigma(V) = \{2.83, 2.83, 2.82, 1.98, 1.41, 0.290, 0.174, 0.021\} \quad (3.14)$$

Since (3.14) indicates that the upper bounds are not small, continue by looking for a set of fault detection filter left eigenvectors that are reasonably well-conditioned. One possible choice has the following singular values

$$\sigma(\tilde{V}) = \{1.46, 1.41, 1.35, 1.00, 1.00, 0.235, 0.056, 0.0028\}$$

Since these singular values are quite close to their respective upper bounds, the detection filter gain should not be large and the filter eigenstructure should not be sensitive to small parameter variations. As in Section 3.1.5, the fault detection filter gain  $L$  is found by solving

$$\tilde{V}^T L = \tilde{W}^T \quad (3.15)$$



where the columns of  $\tilde{V}$  and  $\tilde{W}$  are found from (3.13). Output projection matrices  $\hat{H}_{u_\alpha}$ ,  $\hat{H}_{u_{T_b}}$ ,  $\hat{H}_{y_{m_a}}$  and  $\hat{H}_{y_{T_m}}$  are found in the same way as for the sensor fault example of Section 3.1.5. The filter gain  $L$  and projections  $\hat{H}_{u_\alpha}$ ,  $\hat{H}_{u_{T_b}}$ ,  $\hat{H}_{y_{m_a}}$  and  $\hat{H}_{y_{T_m}}$  are shown in Appendix A

A note should be made regarding the throttle actuator fault residual. By the definition of the complementary faults (3.12),  $F_{u_{T_b}}$  and  $F_{y_{m_a}}$  lie in  $\hat{T}_{u_\alpha}^*$  while  $F_{u_\alpha}$  does not. The effect is that the projected residual is not driven by fault  $F_{u_{T_b}}$  or  $F_{y_{m_a}}$ . Now recall that  $F_{y_{m_a}}$  is a reduced-order approximation for  $E_{y_{m_a}}$  so the throttle actuator residual is not only driven by  $F_{u_\alpha}$ , but also the part of  $E_{y_{m_a}}$  not modeled by  $F_{y_{m_a}}$ . As shown in Figure 3.4, the throttle actuator residual can only isolate faults well at low frequency while other residuals isolate all faults.

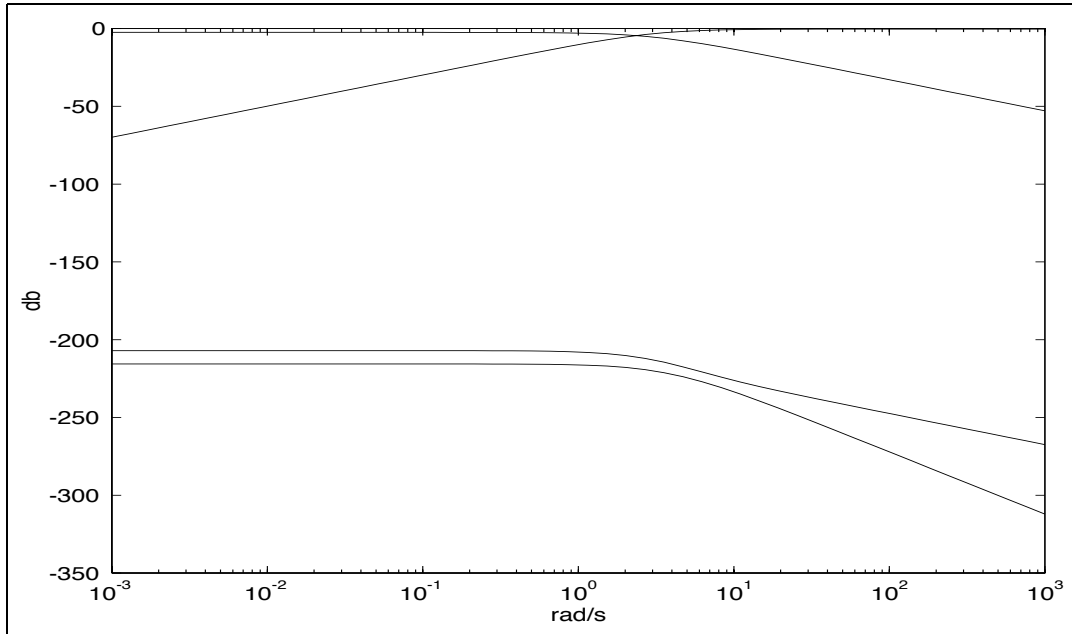


Figure 3.4: Singular value frequency response from all faults to throttle residual.

### 3.2 Algebraic Redundancy

Algebraic parity equations provide a second component to the fault detection and isolation system. The following algebraically redundant pairs are available: the throttle sensor  $y_\alpha$

and throttle actuator, the brake sensor  $y_{T_b}$  and brake actuator  $u_{T_b}$  and the manifold pressure sensor  $y_{pm}$  and manifold air mass sensor  $y_{ma}$ . Three parity equations are defined:

1.  $0 = \text{Throttle sensor } y_\alpha - \text{Throttle actuator } u_\alpha$
2.  $0 = \text{Brake sensor } y_{T_b} - \text{Brake actuator } u_{T_b}$
3.  $0 = \text{Manifold pressure sensor } y_{pm} - \text{Manifold air mass sensor } y_{ma} * 19.9635$

None of the parity equations can by itself identify a fault. But by combining the parity equations with the first fault group detection filter of Section 3.1.4, a unique residual pattern is presented allowing each fault to be isolated. The patterns are summarized in Figure 3.5.

Each row of Figure 3.5 represents a bias (hard) fault in either the throttle actuator, the throttle sensor, the brake actuator, the brake sensor, the manifold air mass sensor, the manifold temperature sensor or the manifold pressure sensor. The columns are the residual responses to the given fault conditions. The first column is the response of the throttle actuator fault residual of the first filter. The second column is the response of the brake actuator fault residual of the first filter. The third column is the response of the air mass sensor and temperature sensor residuals of the first filter. The fourth, fifth and sixth columns are responses of the first, second and third parity equations.

### 3.3 Structure

Combining the fault detection filters of Section 3.1 and parity equations in Section 3.2, a set of six analytic redundancy relationships either dynamic or algebraic are presented. The designs are given in Appendix A.

Fault detection filter 1.

$u_\alpha$  : Throttle actuator.

$u_{T_b}$  : Brake actuator.

$y_{ma}$  : Manifold air mass sensor.

$y_{T_m}$  : Manifold temperature sensor.


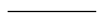
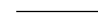






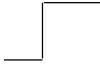










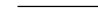
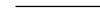



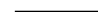










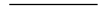
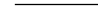




| Residual<br>Fault       | Beard-Jones<br>Fault Detection Filter #1  |   |   | Parity<br>Equation<br>#1   | Parity<br>Equation<br>#2  | Parity<br>Equation<br>#3  |
|-------------------------|---|---|---|--|---|---|
|                         | Throttle<br>Actuator  | Brake<br>Actuator   | Air Mass<br>and<br>Temperature  |  |   |   |
| Throttle<br>Actuator    |    |    |    |    |    |    |
| Throttle<br>Sensor      |    |    |    |    |    |    |
| Brake<br>Actuator       |    |    |    |    |    |    |
| Brake<br>Sensor         |    |    |    |    |    |    |
| Manifold<br>Air Mass    |    |    |    |    |    |    |
| Manifold<br>Temperature |  |  |   |  |  |  |
| Manifold<br>Pressure    |  |  |  |  |  |  |

Figure 3.5: Fault Signatures.

Fault detection filter 2.

$y_{\omega_e}$  : Engine speed sensor.

$y_{a_x}$  : Longitudinal accelerometer.

$y_{\bar{\omega}_f}$  : Sum of front wheel speed sensors.

Fault detection filter 3.

$y_{v_x}$  : Longitudinal velocity sensor.

$y_{a_z}$  : Vertical accelerometer.

$y_{\bar{\omega}_r}$  : Sum of rear wheel speed sensors.

Parity equation 1.

$y_\alpha$  : Throttle sensor.

$u_\alpha$  : Throttle actuator.

Parity equation 2.

$y_{T_b}$  : Brake sensor.

$u_{T_b}$  : Brake actuator.

Parity equation 3.

$y_{pm}$  : Manifold pressure sensor.

$y_{ma}$  : Manifold air mass sensor.

## CHAPTER 4

# Conclusions

---

THIS BRIEF REPORT describes the design of a residual generation system that is a component of a fault detection and identification module in a comprehensive health monitoring and reconfiguration system under development at UC Berkeley. The design illustrates the care that must be taken in forming fault detection filters and parity equations so that each fault produces a unique static pattern. Issues relating to sensor models, output separability, steady-state fault persistence and the spectral content of sensor faults are all considered. Performance evaluation is not done here but a companion report, (Douglas et al. 1997), describes testing done in a high-fidelity vehicle simulation where nonlinearities and road variations are significant. The companion report also describes the design and testing of a residual processor, a multiple hypothesis Shirayev sequential probability ratio test, that examines the filter and parity equation residuals and generates the probability of the presence of a fault.



APPENDIX A

## Fault Detection Filter Design Data

---

THE REDUCED-ORDER longitudinal linearized system matrices used for fault detection filter design are

$$A = \begin{bmatrix} -22.56 & -0.12 & 0 & 0 & 0 & 0 & 0 & 0 \\ 307.03 & -35.41 & 396.80 & -2698.58 & -238.10 & 1901.28 & -432.86 & -0.08 \\ 0 & 0.07 & -0.76 & 4.87 & 0.43 & -3.29 & 0.87 & -0.00 \\ 0 & 0 & 0.00 & 0 & 1.00 & -25.00 & 0 & 0 \\ 0 & -0.00 & -0.01 & -39.72 & -3.50 & 78.91 & 24.20 & 0.00 \\ 0 & 0 & 0 & 0 & 0 & 0 & 1.00 & 0 \\ 0 & -0.02 & 0.22 & -7.19 & -0.61 & -25.26 & -3.73 & 0.00 \\ 0 & 0 & 0 & 0 & 0 & 0 & 0 & -1.25 \end{bmatrix}$$

$$B = \begin{bmatrix} 2.35 & 0 & -0.12 \\ 0 & 0 & 1.66 \\ 0 & 0 & 0 \\ 0 & 0 & 0 \\ 0 & 0 & 0 \\ 0 & 0 & 0 \\ 0 & 0 & 0 \\ 0 & 1.25 & 0 \end{bmatrix}$$

$$C = \begin{bmatrix} 1.00 & 0 & 0 & 0 & 0 & 0 & 0 & 0 \\ 0 & 1.00 & 0 & 0 & 0 & 0 & 0 & 0 \\ 0 & 0 & 1.00 & 0 & 0 & 0 & 0 & 0 \\ 0 & 0.07 & -0.76 & 4.87 & 0.43 & -3.29 & 0.87 & -0.00 \\ 0 & -0.00 & -0.01 & -39.72 & -3.50 & 78.91 & 24.20 & -0.00 \\ 0 & 0 & 7.10 & -45.34 & -4.00 & 146.48 & 2.83 & -0.00 \\ 0 & 0.09 & 5.96 & -40.56 & -3.58 & 28.58 & -6.51 & -0.00 \end{bmatrix}$$

$$D = \begin{bmatrix} 0 & 0 & 0 \\ 0 & 0 & 0 \\ 0 & 0 & 0 \\ 0 & 0 & 0 \\ 0 & 0 & 0 \\ 0 & 0 & 0 \\ 0 & 0 & 0 \end{bmatrix}$$

The filter gain  $L$  and the output projection matrices  $\hat{H}_{u_\alpha}$ ,  $\hat{H}_{u_{T_b}}$ ,  $\hat{H}_{y_{m_a}}$  and  $\hat{H}_{y_{T_m}}$  for the first fault detection filter are as follows.

$$L = \begin{bmatrix} 19.56 & 0.12 & 0.00 & 0.00 & -0.00 & -0.00 & 0.00 \\ -307.03 & 523.06 & -334.41 & -6277.18 & 8.39 & 3.99 & -832.46 \\ -0.00 & 11.97 & -11.36 & -156.00 & 0.20 & 0.10 & -18.91 \\ 0.00 & 0.00 & -1.96 & -0.10 & -0.06 & 0.19 & 0.03 \\ 0.00 & -0.07 & -7.21 & -0.00 & -1.17 & -0.08 & 0.83 \\ -0.00 & -0.00 & 0.01 & -0.01 & -0.02 & -0.02 & 0.03 \\ 0.00 & -3.51 & 1.38 & 46.16 & -0.26 & 0.32 & 5.26 \\ -0.00 & -60.65 & 19.39 & 784.64 & -2.29 & 0.07 & 96.37 \end{bmatrix}$$

$$\hat{H}_{u_\alpha} = \begin{bmatrix} 0.93 & 0.07 & -0.02 & 0.11 & 0.16 & -0.10 & -0.11 \\ 0.07 & 0.01 & -0.00 & 0.01 & 0.00 & 0.03 & -0.05 \\ -0.02 & -0.00 & 0.99 & 0.04 & 0.05 & -0.03 & -0.04 \\ 0.11 & 0.01 & 0.04 & 0.16 & -0.28 & -0.12 & -0.18 \\ 0.16 & 0.00 & 0.05 & -0.28 & 0.62 & 0.23 & 0.28 \\ -0.10 & 0.03 & -0.03 & -0.12 & 0.23 & 0.73 & -0.35 \\ -0.11 & -0.05 & -0.04 & -0.18 & 0.28 & -0.35 & 0.55 \end{bmatrix}$$

$$\hat{H}_{u_{T_b}} = \begin{bmatrix} 0 & 0.00 & 0 & 0.00 & -0.00 & 0 & 0.00 \\ 0.00 & 0.01 & 0 & -0.07 & 0.00 & 0 & -0.09 \\ 0 & 0 & 1.00 & 0 & 0 & 0 & 0 \\ 0.00 & -0.07 & 0 & 1.00 & 0.00 & 0 & -0.01 \\ -0.00 & 0.00 & 0 & 0.00 & 1.00 & 0 & 0.00 \\ 0 & 0 & 0 & 0 & 0 & 1.00 & 0 \\ 0.00 & -0.09 & 0 & -0.01 & 0.00 & 0 & 1.00 \end{bmatrix}$$



$$\hat{H}_{y_{m_a}} = \hat{H}_{y_{T_m}} = \begin{bmatrix} 0 & 0 & 0 & 0 & 0 & 0 & 0 \\ 0 & 0.08 & -0.02 & 0.13 & 0.16 & -0.07 & -0.16 \\ 0 & -0.02 & 1.00 & 0.00 & 0.00 & -0.00 & -0.00 \\ 0 & 0.13 & 0.00 & 0.35 & -0.02 & -0.28 & -0.36 \\ 0 & 0.16 & 0.00 & -0.02 & 0.97 & 0.01 & 0.03 \\ 0 & -0.07 & -0.00 & -0.28 & 0.01 & 0.86 & -0.19 \\ 0 & -0.16 & -0.00 & -0.36 & 0.03 & -0.19 & 0.74 \end{bmatrix}$$

The filter gain  $L$  and the output projection matrices  $\hat{H}_{y_{\omega_e}}$ ,  $\hat{H}_{y_{a_x}}$ ,  $\hat{H}_{y_{\omega_f}}$  for the second fault detection filter are as follows.

$$L = \begin{bmatrix} 18.56 & 0.12 & -0.00 & 0.00 & 0.00 & -0.00 & 0.00 \\ -307.03 & 38.32 & -0.00 & -0.00 & -0.00 & 0.00 & -66.53 \\ 0.01 & -0.00 & -3.00 & -1.00 & 0.00 & 0.00 & 0.00 \\ 0.75 & 0.01 & 0.16 & -0.04 & 0.04 & 0.21 & -0.13 \\ 2.16 & -0.00 & 4.11 & -0.01 & -0.61 & -0.00 & -0.08 \\ -0.01 & -0.00 & -0.13 & -0.02 & -0.03 & -0.02 & 0.05 \\ 0.54 & 0.03 & 0.02 & 0.36 & -0.12 & 0.33 & -0.38 \\ 0.01 & -95.97 & 32.35 & 1230.72 & -3.58 & 0.10 & 151.14 \end{bmatrix}$$

$$\hat{H}_{y_{\omega_e}} = \begin{bmatrix} 1.00 & -0.00 & -0.00 & 0.00 & 0.00 & -0.00 & -0.00 \\ -0.00 & 1.00 & -0.00 & 0.00 & 0.00 & 0.00 & -0.00 \\ -0.00 & -0.00 & 0.99 & 0.00 & 0.09 & -0.00 & -0.02 \\ 0.00 & 0.00 & 0.00 & -0.00 & 0.00 & -0.00 & -0.00 \\ 0.00 & 0.00 & 0.09 & 0.00 & 0.01 & -0.00 & -0.00 \\ -0.00 & 0.00 & -0.00 & -0.00 & -0.00 & 0.00 & 0.00 \\ -0.00 & -0.00 & -0.02 & -0.00 & -0.00 & 0.00 & 0.00 \end{bmatrix}$$

$$\hat{H}_{y_{a_x}} = \begin{bmatrix} 1.00 & 0.00 & 0.00 & -0.04 & 0.06 & -0.00 & -0.06 \\ 0.00 & 0.00 & -0.00 & 0.00 & 0.00 & -0.00 & -0.00 \\ 0.00 & -0.00 & 1.00 & 0.00 & -0.00 & -0.00 & 0.00 \\ -0.04 & 0.00 & 0.00 & 0.03 & 0.18 & -0.00 & -0.03 \\ 0.01 & 0.00 & -0.00 & 0.18 & 0.94 & -0.00 & -0.17 \\ -0.00 & -0.00 & -0.00 & -0.00 & -0.00 & 0.00 & 0.00 \\ -0.01 & -0.00 & 0.00 & -0.03 & -0.17 & 0.00 & 0.03 \end{bmatrix}$$

$$\hat{H}_{y_{\omega_f}} = \begin{bmatrix} 1.00 & -0.00 & 0.00 & 0.00 & -0.01 & 0.03 & -0.04 \\ -0.00 & -0.00 & -0.00 & -0.00 & 0.00 & 0.00 & 0.00 \\ 0.00 & -0.00 & 0.99 & 0.00 & 0.05 & -0.05 & -0.02 \\ 0.00 & -0.00 & 0.00 & 0.00 & -0.00 & -0.00 & -0.00 \\ -0.01 & 0.00 & 0.05 & -0.00 & 0.58 & 0.47 & 0.15 \\ 0.03 & 0.00 & -0.05 & -0.00 & 0.47 & 0.39 & 0.12 \\ -0.04 & 0.00 & -0.02 & -0.00 & 0.15 & 0.12 & 0.04 \end{bmatrix}$$

The filter gain  $L$  and the output projection matrices  $\hat{H}_{y_{vx}}$ ,  $\hat{H}_{y_{\alpha z}}$ ,  $\hat{H}_{y_{\omega_f}}$  for the third fault detection filter are as follows.

$$L = \begin{bmatrix} 1.96 & 0.12 & -0.00 & 0.00 & -0.00 & -0.00 & 0.00 \\ -307.03 & 38.32 & -0.00 & 0.01 & -0.00 & 0.00 & -66.53 \\ -0.00 & 0.00 & -3.01 & -1.01 & 0.00 & -0.00 & 0.00 \\ 0.00 & 0.07 & -1.11 & -0.52 & -0.06 & 0.34 & -0.10 \\ 0.00 & 0.38 & -0.02 & -3.38 & -1.14 & 0.56 & 0.01 \\ -0.00 & -0.00 & -0.24 & -0.06 & -0.03 & -0.04 & 0.05 \\ 0.00 & 0.03 & 0.26 & 0.39 & -0.15 & 0.36 & -0.35 \\ 0.00 & -94.97 & 14.68 & 1234.19 & -3.10 & 1.68 & 151.15 \end{bmatrix}$$

$$\hat{H}_{y_{vx}} = \begin{bmatrix} 1.00 & -0.00 & -0.00 & 0.00 & -0.00 & -0.00 & 0.00 \\ -0.00 & 0.00 & -0.00 & -0.03 & 0.00 & -0.01 & 0.00 \\ -0.00 & -0.00 & 1.00 & 0.00 & -0.00 & -0.00 & 0.00 \\ 0.00 & -0.03 & 0.00 & 0.90 & -0.00 & 0.30 & -0.00 \\ -0.00 & 0.00 & -0.00 & -0.00 & -0.00 & -0.00 & -0.00 \\ -0.00 & -0.01 & -0.00 & 0.30 & -0.00 & 0.10 & -0.00 \\ 0.00 & 0.00 & 0.00 & -0.00 & -0.00 & -0.00 & -0.00 \end{bmatrix}$$

$$\hat{H}_{y_{\alpha z}} = \begin{bmatrix} 1.00 & 0.00 & 0.00 & 0.00 & -0.00 & 0.00 & 0.00 \\ 0.00 & 0.03 & -0.00 & -0.08 & 0.02 & 0.16 & -0.00 \\ 0.00 & -0.00 & -0.00 & 0.00 & -0.00 & -0.00 & -0.00 \\ 0.00 & -0.08 & 0.00 & 0.99 & 0.07 & 0.00 & 0.00 \\ -0.00 & 0.02 & -0.00 & 0.07 & 0.03 & 0.16 & -0.00 \\ 0.00 & 0.15 & -0.00 & 0.00 & 0.16 & 0.95 & -0.00 \\ 0.00 & -0.00 & -0.00 & 0.00 & -0.00 & -0.00 & -0.00 \end{bmatrix}$$

$$\hat{H}_{y_{\omega_f}} = \begin{bmatrix} 1.00 & -0.00 & 0.00 & -0.00 & -0.00 & 0.0 & 0.00 \\ -0.00 & 1.00 & 0.00 & -0.00 & 0.00 & 0.00 & 0.00 \\ 0.00 & 0.00 & -0.00 & -0.00 & -0.00 & -0.00 & -0.00 \\ -0.00 & -0.00 & -0.00 & 0.99 & -0.00 & 0.01 & 0.12 \\ -0.00 & 0.00 & -0.00 & -0.00 & 0 & -0.00 & -0.00 \\ 0.00 & 0.00 & -0.00 & 0.01 & -0.00 & 0.00 & 0.00 \\ 0.00 & 0.00 & -0.00 & 0.12 & -0.00 & 0.00 & 0.01 \end{bmatrix}$$

## References

---

- Douglas, R. K. 1993. *Robust Fault Detection Filter Design*. PhD thesis, The University of Texas at Austin, Austin, TX.
- Douglas, R. K., W. H. Chung, D. P. Malladi, R. H. Chen, J. L. Speyer, and D. L. Mingori 1997. Integration of Fault Detection and Identification into a Fault Tolerant Automated Highway System: Final Report. Research report for mou 291, University of California, Los Angeles, MAE Dept. and California PATH.
- Douglas, R. K., J. L. Speyer, D. L. Mingori, R. H. Chen, D. P. Malladi, and W. H. Chung 1996. Fault Detection and Identification with Application to Advanced Vehicle Control Systems: Final Report. Research Report UCB-ITS-PRR-96-25, University of California, Los Angeles, MAE Dept. and California PATH.
- Massoumnia, M.-A. 1986. A Geometric Approach to the Synthesis of Failure Detection Filters. *IEEE Transactions on Automatic Control*, Vol. AC-31, No. 9:839–846.
- White, J. E. and J. L. Speyer 1987. Detection Filter Design: Spectral Theory and Algorithms. *IEEE Transactions on Automatic Control*, Vol. AC-32, No. 7:593–603.